energies

MDPI

Article

Conceptual Design of an Energy System for High Altitude Airships Considering Thermal Effect

Qiumin Dai [1,*], Daoming Xing [1], Xiande Fang [2] and Yingjie Zhao [3]

[1] School of Energy and Power Engineering, Nanjing University of Science and Technology, Nanjing 210094, China; hingdaoming@163.com
[2] MIIT Key Laboratory of Aircraft Environment Control and Life Support, Nanjing University of Aeronautics and Astronautics, Nanjing 210016, China; xd_fang@nuaa.edu.cn
[3] College of Energy and Power Engineering, Jiangsu University of Science and Technology, Zhenjiang 212003, China; lszhaoyingjie@126.com
* Correspondence: daiqiumin@njust.edu.cn; Tel.: +86-13770960667

Abstract: High altitude airships possess tremendous potential for long-endurance spot hovering platforms for both commercial and strategic applications. The energy system, which is mainly made up of solar array and regenerative fuel cell, is the key component of a high altitude airship. The thermal effect is a major factor that affects the performance of the energy system of long endurance stratospheric vehicles. In this paper, a conceptual design method focusing on the thermal and power characteristics of an energy system for stratospheric airships is proposed. The effect of thermal behavior of solar array on the energy system is analyzed. An optimized case is obtained on the consideration of power supply, thermal behaviors of helium and solar array. Results show that the maximum temperature difference of the solar array may be reduced by about 20 K and the mass of payload can be improved by up to 5%.

Keywords: high altitude airships; energy system; solar array; thermal-electric model

Citation: Dai, Q.; Xing, D.; Fang, X.; Zhao, Y. Conceptual Design of an Energy System for High Altitude Airships Considering Thermal Effect. *Energies* **2021**, *14*, 4204. https://doi.org/10.3390/en14144204

Academic Editor: Adrian Ilinca

Received: 17 May 2021
Accepted: 9 July 2021
Published: 12 July 2021

1. Introduction

The high altitude airship (HAA) is a lighter-than-air vehicle whose lift is mainly derived from the contained buoyancy gas. With the capability of spot hovering in the stratosphere for more than one year, the HAA can be treated as an ideal persist stratospheric platform for ground surveillance [1], telecommunication [2], and military applications [3]. Due to the growing application prospect, the HAA has drawn increasing attentions from all over the world in the recent decades.

Due to the requirement of long duration in the stratosphere, the energy system is the key component of HAAs. One of the most popular ideas for the energy system is the solar array–regenerative fuel cell system, which commonly includes a flexible solar array, regenerative fuel cell (RFC), and other ancillary components [4]. In the daytime, HAAs harvest solar energy from the solar array mounted on the upper envelope. Part of the electric energy is directly supplied to the propulsion system, onboard payload, and other electric equipment. The rest is stored in the RFC for nighttime consumption.

A series of research activities have been carried out on the energy system of HAAs in the last decade. Some of the researches focus on the solar array, including the thermal management, estimation of the power output of the solar array, and optimization of the required solar array area. Garg et al. estimated and optimized the area of a solar array based on an analytic method [5]. Liu et al. proposed a comprehensive model to analyze the temperature distribution and flow field of the airship [6]. The effect of the solar array on the thermal performance of the airship was studied. Li et al. used their analytical method to evaluate the effect of wind velocity and glass cover transmissivity on the thermal and power characteristics of a solar powered airship [7]. Then, the optimized distribution

of a solar array on a stratospheric airship was designed. Alam and Pant presented a method for minimizing the area of a solar array by optimizing the envelope shape [8]. The variables related to environment, geometry, aerodynamics, and energy were involved in the methodology. Kayhan outlined a numerical model in which the effects of thermal characteristics, solar radiation, and power output were considered [9]. Zhu et al. studied the effect of layout parameters on the power output of the solar array. Then the distribution of the solar array was optimized under the consideration of thermal effect. Meanwhile, the power output of the solar array was studied through optimizing the transmittance of solar array encapsulant [10,11]. Wang et al. accurately predicted the operating temperature of the solar array on a stratospheric airship by using a support vector machine prediction method based on the particle swarm optimization algorithm [12].

While other researches aimed to design and optimize the entire energy system, including the total mass of the energy system, energy balance between solar array and RFC, and the balance between energy acquisition and consumption, Colozza and Dolce carried out a feasibility study on the energy supply for HAAs [13]. The study provided an outstanding design idea and complete computing method. Knaupp and Mundschau investigated the power supply for an airship at stratosphere and proposed the design scheme of the energy system [14]. Li et al. proposed a novel RFC system with low pressure gasbags in which hydrogen and oxygen were stored [15]. Based on the weight and energy balances, they established the general parameters of the airships. Smith et al. proposed a new concept energy system of the all-electric airships. Specific focus is given to the cloud albedo effects on the solar array [16]. Yang and Liu proposed a conceptual design method to achieve the energy and mass balances for stratospheric airships [17]. The effects of geometry, aerodynamics, propulsion, and renewable fuel cell on the energy system were considered in the method.

From the above introduction, it can be seen that thermal effect on the energy supply system of an airship has rarely been considered. To enrich the previous research, a thermo-electric model is established to study the thermal and power output behaviors of solar arrays in this paper. The conceptual design and optimization process for energy supply is addressed. The thermal effect on the power output of a solar array is simulated and discussed in detail. The results may provide guidance for the design and management of the energy system for high altitude airships.

2. Methodology

As is shown in Figure 1, the power output of a HAA is a complex thermal-electric coupling process. In order to better analyze the power output behaviors and design the energy supply system, a coupled thermal-energy model should be developed.

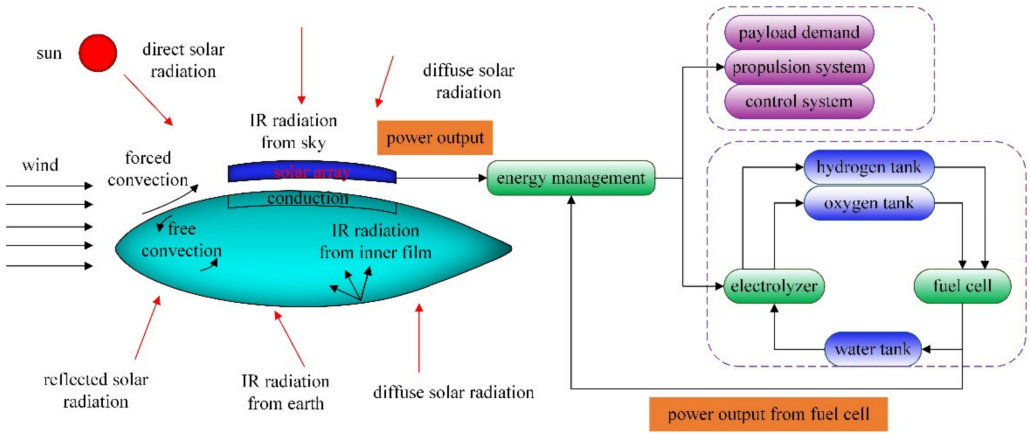

Figure 1. Thermal-electric coupled process of HAAs.

2.1. Thermal Model

In order to overcome the weight of payload, the stratospheric airship possesses a huge volume. Affected by solar radiation and IR radiation, there are evident temperature gradients on the envelope and solar array. Therefore, both the solar array and the envelope are divided into triangle flat elements with similar area to demonstrate the temperature distribution. Meanwhile, the heat transfer between the triangle flat elements can be neglected because of the thickness of envelope and solar array. Thus, a spatially distributed thermal model can be applied in determining the thermal characteristics of triangle flat elements.

2.1.1. Thermal Model of Solar Array

The transient heat balance equation of the ith solar array element can be written as

$$M_{sa,i}c_{sa}\frac{\mathrm{d}T_{sa,i}}{\mathrm{d}t} = Q_{sa,solar,i} + Q_{sa,ir,i} + Q_{sa,conv,i} - Q_{sa,cond,i} - P_{sa,i} \tag{1}$$

where $M_{sa,i}$ is the mass of the ith solar array element, c_{sa} is the specific heat of solar array, $T_{sa,i}$ is the temperature of the ith solar array element. $Q_{sa,solar,i}$, $Q_{sa,ir,i}$, $Q_{sa,conv,i}$, $Q_{sa,cond,i}$, and $P_{sa,i}$ are the solar radiation heat load, IR heat load, convection heat load, heat conduction between solar cells and film, and power output of the ith solar array element, respectively.

The solar radiation heat load of the ith solar array element can be given by

$$Q_{sa,solar,i} = \alpha_{sa}\tau_{glass}A_{sa,i}(q_{sa,D,i} + q_{sa,S,i} + q_{sa,R,i}) \tag{2}$$

where α_{sa} is the solar absorptivity of solar array, τ_{glass} is the transmittance of glass cover of solar array element and $A_{sa,i}$ is the area of the ith solar array element. $q_{sa,D,i}$, $q_{sa,S,i}$, and $q_{sa,R,i}$ are incident solar radiation flux from direct, diffuse, and reflected solar radiation on the ith solar array element, respectively.

The direct incident solar radiation flux of element i can be given by

$$q_{sa,D,i} = \delta I_D \cos\theta_{sa,i} \tag{3}$$

where I_D is the direct solar intensity, $\theta_{sa,i}$ is the included angle between sunlight and the normal of the ith solar array element, and δ is the projection coefficient of direct solar radiation on the element. If $\theta_{sa,i}$ is an obtuse angle, $\delta = 1$. Otherwise, $\delta = 0$.

The diffuse solar radiation flux on the element of element i can be written as

$$q_{sa,S,i} = I_S\varphi_{sa,i} \tag{4}$$

$$q_{sa,R,i} = I_R(1 - \varphi_{sa,i}) \tag{5}$$

where I_S and I_R are diffuse and reflected solar intensity, $\varphi_{sa,i}$ is the view factor from the ith solar array element to the sky, it can be calculated from [18].

The IR heat load of the ith solar array element can be written as

$$Q_{sa,ir,i} = \underbrace{\varepsilon_{sa}A_{sa,i}\left(E_{sky} - \sigma T_{sa,i}^4\right)\varphi_{sa,i}}_{IR\ between\ atmosphere} + \underbrace{\varepsilon_{sa}A_{sa,i}\left(E_g - \sigma T_{sa,i}^4\right)(1 - \varphi_{sa,i})}_{IR\ between\ ground} \tag{6}$$

where ε_{sa} is the IR emissivity of solar array, σ is the Stefan-Boltzmann constant, E_{sky} is the downward infrared radiation from atmosphere, and E_g is the upward infrared radiation from the earth.

The convection heat load of the ith solar array element can be calculated by

$$Q_{sa,conv,i} = h_{sa,ce,i}A_{sa,i}(T_a - T_{sa,i}) \tag{7}$$

where $h_{sa,ce,i}$ is the external forced convection heat transfer coefficient of the ith solar array element, Ta is the ambient temperature.

The heat conduction between solar cells and film can be described as

$$Q_{sa,cond,i} = A_{sa,i}(T_{sa,i} - T_{en,i})/R \tag{8}$$

where R is the thermal resistance between solar array element and the envelope below, T_{en} is the temperature of the envelope blow solar array.

2.1.2. Thermal Model of Envelope

Affected by the solar array mounted on the top of the airship, the envelope can be divided into the bare envelope and the envelope below the solar array.

The transient energy balance equation of bare envelope element is calculated by

$$M_{en,i}c_{en}\frac{\mathrm{d}T_{en,i}}{\mathrm{d}t} = Q_{en,solar,i} + Q_{en,ir,i} + Q_{en,conv,i} \tag{9}$$

where $M_{en,i}$ is the mass of envelope element, c_{en} is the specific heat of envelope. $Q_{en,solar,i}$, $Q_{en,ir,i}$, and $Q_{en,conv,i}$ are the solar radiation heat load, IR heat load, and convection heat load of the ith envelope element, respectively.

The solar radiation heat load of envelope element is calculated by

$$Q_{en,solar,i} = \alpha_{en}A_{en,i}(q_{en,D,i} + q_{en,S,i} + q_{en,R,i}) \tag{10}$$

where α_{en} is the solar absorptivity of the envelope, $A_{en,i}$ is the area of the ith envelope element. $q_{en,D,i}$, $q_{en,S,i}$, and $q_{en,R,i}$ are incident solar radiation flux from direct, diffuse, and reflected solar radiation on the ith envelope element, respectively.

The IR heat load of envelope element can be written as

$$\begin{aligned} Q_{en,ir,i} = {} & \underbrace{\varepsilon_{en}A_{en,i}\left(E_{sky} - \sigma T_{en,i}^4\right)\varphi_{en,i}}_{IR\ with\ atmosphere} + \underbrace{\alpha_{en}A_{en,i}\left(E_g - \sigma T_{en,i}^4\right)(1-\varphi_{en,i})}_{IR\ with\ atmosphere} \\ & + \underbrace{A_{en,i}(G_{en,i} - J_{en,i})}_{inner\ IR} \end{aligned} \tag{11}$$

where ε_{en} is the infrared radiation emissivity of the envelope, $\varphi_{sa,i}$ is the view factor from the ith envelope element to the sky, $G_{en,i}$ is the IR falling on the element and $J_{en,i}$ is the IR away from the ith envelope element.

The convection heat load of bare envelope element is written as

$$Q_{en,conv,i} = h_{en,ce,i}A_{en,i}(T_a - T_{en,i}) + h_{en,ci,i}A_{en,i}(T_{he} - T_{en,i}) \tag{12}$$

where T_{he} is the temperature of helium. $h_{en,ce,i}$ and $h_{en,ci,i}$ are the external forced and internal natural convection heat transfer coefficient of the ith envelope element.

If the envelope element is located below the solar array, the forced convection heat transfer between atmosphere and IR between atmosphere and ground can be ignored. Then Equation (9) can be simplified as

$$M_{en,i}c_{en}\frac{\mathrm{d}T_{en,i}}{\mathrm{d}t} = Q_{en,conv,i} + Q_{sa,cond,i} \tag{13}$$

The convection heat load of envelope element below solar array can be written as

$$Q_{en,conv,i} = h_{en,ci,i}A_{en,i}(T_{he} - T_{en,i}) \tag{14}$$

2.1.3. Thermal Model of Buoyancy Gas

It is assumed that the buoyancy gas in the airship ballonet is transparent to solar and IR radiation. Then the thermal balance equation of the airship at stratosphere can

be derived from the energy equation of a closed system. The helium temperature can be calculated by

$$M_{he}c_{he}\frac{\mathrm{d}T_{he}}{\mathrm{d}t} = \sum h_{en,ci,i}A_{en,i}(T_{en,i} - T_{he}) \tag{15}$$

where M_{he} is the mass of helium and c_{he} is the specific heat of helium at constant volume.

2.2. Power Output of Solar Array

The power output of solar array is dominated by the incident solar intensity and the photoelectric conversion efficiency of solar array. The power generated by the solar array element can be written as

$$P_{sa,i} = \tau_{glass}(q_{sa,D,i} + q_{sa,S,i} + q_{sa,R,i})A_{sa,i}\eta_{T,i} \tag{16}$$

where $\eta_{T,i}$ is the efficiency of the ith solar array element. It varies with temperature and is defined as

$$\eta_{T,i} = \eta_{ref}\left[1 - \beta\left(T_{sa,i} - T_{ref}\right)\right] \tag{17}$$

where the reference temperature T_{ref} is 288 K, the electrical efficiency at reference temperature ¦ η_{ref} is 0.127, and β is temperature coefficient having value of 0.0045/K [19].

2.3. Constraints

The electric energy generated by the solar array should satisfy the energy consumed by the airship all day and the storage energy in the RFC should support the energy consumption in the nighttime. In addition, according to the principle of aerostatics, the total weight of the airship cannot exceed the net buoyancy.

2.3.1. Energy Constraints

The total energy generated by solar array in a day is calculated by

$$Es = \int_{t\_rise}^{t\_set} \sum P_{sa,i}dt \tag{18}$$

where *t_rise* is the time of sunrise and *t_set* is the time of sunset.

The total energy requirement of the airship consists of energy consumed by control system, the payload, and the propulsion system. The total energy consumed by the airship throughout a day *Ec* can be calculated by

$$Ec = \int_{1day} k\left(P_{pro} + P_{con} + P_{pay}\right)dt \tag{19}$$

where κ is the safe coefficient, κ = 1.2. P_{pro}, P_{con}, and P_{pay} are the power required by the propulsion system, control system, and payload, respectively. The energy consumed by the propulsion system, control system and payload on the winter solstice at 20 km when the wind speed is 15 m/s is shown in Figure 2.

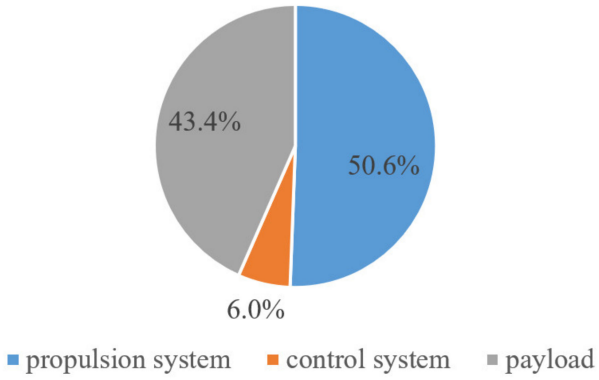

Figure 2. The proportion of energy consumption.

The process of energy generation and consumption in a day can be seen in Figure 3. According to the energy constraints, the total energy generated by the solar array *Es* should be greater than the total energy consumed by the airship. Moreover, the storage energy *Estore* in the daytime should be greater than the consumption energy provided by the RFC during nighttime. The relations of energy constraints can be written as

$$\begin{cases} Es > Ec \\ \eta_{ef} Estore > Ef \end{cases} \tag{20}$$

where *Es* is the total energy consumed by airship, *Ef* is the energy consumption during nighttime, and η_{ef} is the electrical efficiency of the RFC.

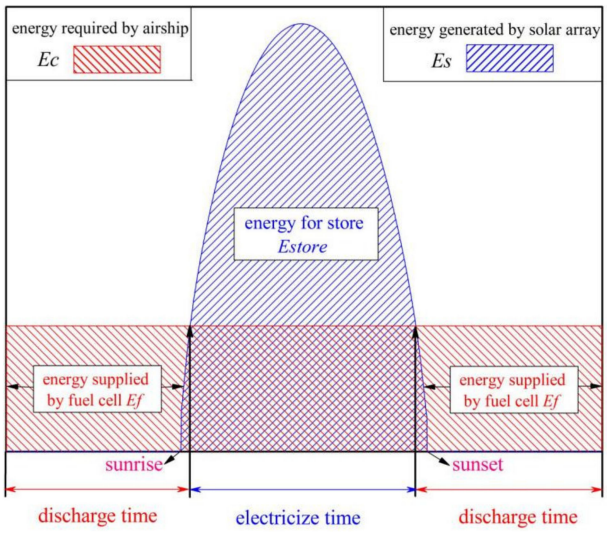

Figure 3. The process of energy balance.

2.3.2. Mass Constraints

Since the airship is operated by net buoyancy, weight constraints should be considered in the design of airship. The maximum inflight mass m_{max} can be calculated as following:

$$m_{max} = (\rho_a - \rho_{he})V \tag{21}$$

where ρ_a is the ambient air density, ρ_{he} is the helium density, and V is the volume of the airship.

The maximum inflight mass is expressed as

$$m_{max} > m_{str} + m_{RFC} + m_{pro} + m_{pay} \tag{22}$$

where m_{str} is the mass of airship structure, m_{RFC} is the mass of RFC, m_{pro} is the mass of propulsion system, and m_{pay} is the mass of payload.

The mass of airship is calculated as

$$m_{str} = \rho_{en} \sum A_{en,i} + \rho_{sa} \sum A_{sa,i} \tag{23}$$

where ρ_{en} is the area density of the envelope, ρ_{sa} is the area density of the solar array.

The mass of RFC can be determined by

$$m_{RFC} = Ef/\omega_{RFC} \tag{24}$$

where ω_{RFC} is the energy density of RFC system.

The mass of propulsion system mass can be determined according to the volume and drag coefficient of the airship.

3. Method

Based on the theory described above, a method was proposed to design an optimized energy supply system of stratospheric airship. The detailed process is described in Figure 4. It is clear that the thermal behaviors of the airship interact with the performance of the solar array.

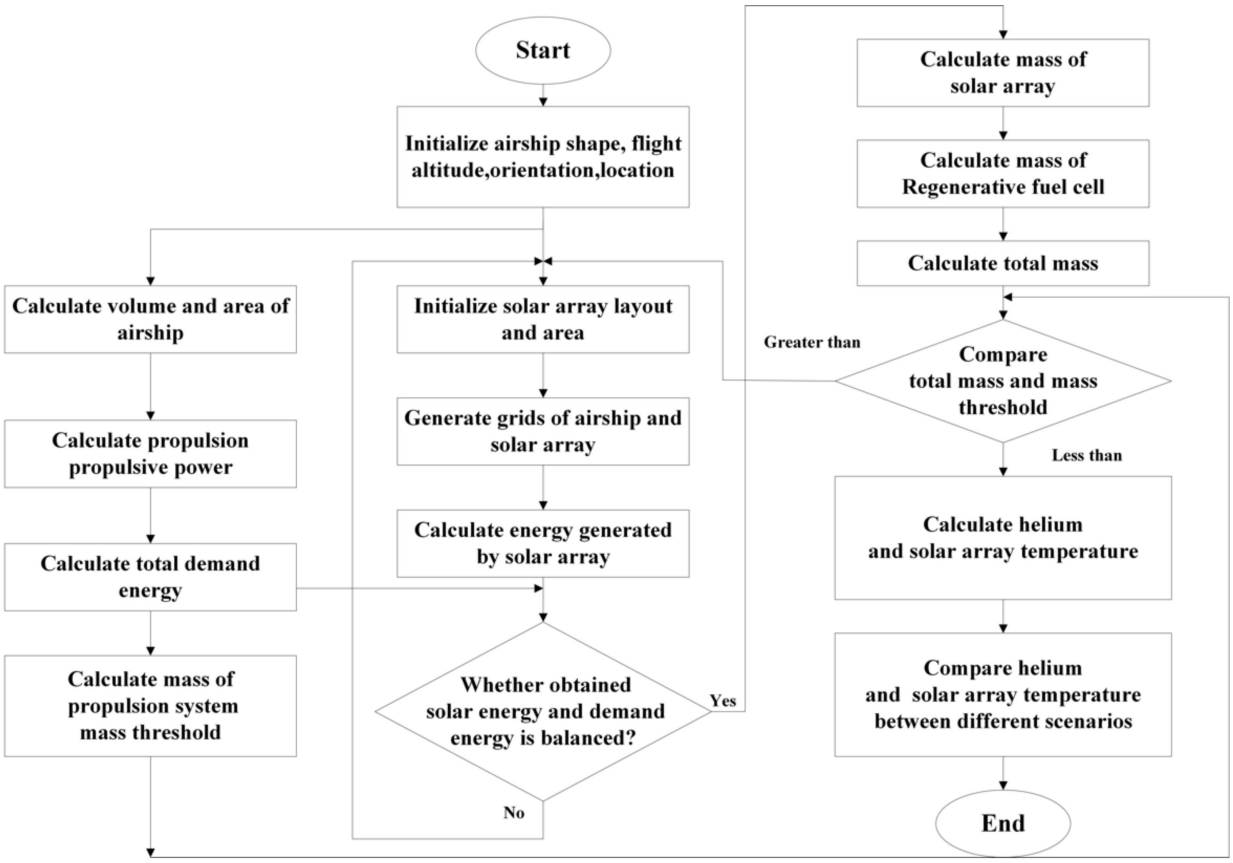

Figure 4. The design process of energy supply system for a HAA.

The governing equations of the thermal model are traditional ordinary differential equations and can be discretized by the Runge-Kutta method. The envelope of the stratospheric airship was divided into 3778 flat triangular elements, while the solar array was separated into 1074 elements. Therefore, a simulation code programmed in FORTRAN95 with the in-house developed standard fourth-order adaptive-step Runge-Kutta method was developed to estimate the thermal characteristics of the airship and evaluate the power

balance of the energy system. The simulation code can numerically solve the un-coupled ordinary differential equations simultaneously. According to the maximum temperature variation rate of the envelope and the solar array, the time step adopted in the code varies from 0.1 to 1 s.

The temperatures of the airship (including envelope, solar array and helium) were assumed to be equal to the ambient temperature. Then, the thermal characteristics of the airship were calculated according to the surrounding environment from 22:00, which was 2 h before the thermal characteristics were recorded and analyzed. It was found that, after 2 h' exposure in the ambient environment, the real temperatures of the envelope and the solar array were stable at 00:00 and could be adopted as the initial conditions for the daily simulation [20].

The accuracy and feasibility of the thermal model and simulation code has been verified by the experiment results of a 35 m-long PV-equipped airship tested by Harada et al. in our previous paper [18,20].

4. Results and Discussion

The design parameters of the airship are listed in Table 1. The daily energy consumption is about 6.11 GJ. In order to verify the feasibility of long endurance, winter solstice, which indicates the poorest solar condition, was adopted in this paper.

Table 1. Design parameters of the HAA.

Parameter	Values
Length	152.4 m
Aspect ratio	3.5
Volume	132,000 m^3
Envelope area	15,200 m^2
Solar absorptivity of envelope	0.15
Infrared emissivity of envelope	0.8
Area density of envelope	0.1 kg/m^2
Location	32° N, 118° E
Height	20 km
Orientation	West
Wind speed	20 m/s
Solar absorptivity of solar array	0.93
Infrared emissivity of solar array	0.9
Area density of solar array	1.0 kg/m^2
Transmittance of glass cover	0.95
Propulsive efficiency	80%
Propulsion system power density	130 W/kg
Electrical efficiency of RFC	53.4%
RFC energy density	790 W·h/kg

4.1. Thermal Effect on the Power Output

A preliminary case for the solar array layout was designed according to the conventional design experience. The solar array mounted on the top of the envelope was located from 0.3 to 0.7 *L* of the airship length. The central angle of the solar array was adjusted to generate sufficient energy to meet the energy consumption (shown in Figure 5). It can be seen in Table 2 that the scheme of the central angle larger than 130° under the length layout meets the daily energy consumption. Therefore, the case with the 3055 m^2 solar array is adopted. In addition, the thermal effect on the energy supplied by the solar array can also be seen from Table 2.

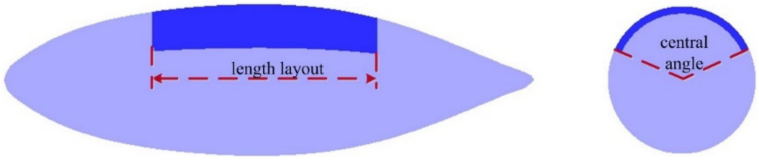

Figure 5. Schematic diagram of the solar array layout.

Table 2. Energy generated by the solar array on the winter solstice.

Central Angle and Area	Energy (GJ) With Thermal Effect		Energy (GJ) Without Thermal Effect
	α_{sa} = 0.93	α_{sa} = 0.6	
60°, 1375 m^2	2.98	3.32	2.75
80°, 1867 m^2	3.91	4.40	3.71
90°, 2115 m^2	4.40	4.96	4.22
100°, 2362 m^2	4.89	5.54	4.74
110°, 2609 m^2	5.38	6.12	5.28
120°, 2820 m^2	5.81	6.62	5.74
130°, 3055 m^2	6.28	7.18	6.26
150°, 3523 m^2	7.24	8.30	7.30
180°, 4228 m^2	8.63	9.91	8.80

As mentioned in Table 2, the solar array with 130° central angle and 3055 m^2 solar array area was applied to evaluate the thermal effect on the energy generation on the winter solstice. The thermal effect on the power output of the solar array on the winter solstice is shown in Figure 6. From sunrise to 9:40 and 14:11 to sunset, the actual power output considering thermal effect is larger than that of the conventional method. While the actual power output of the solar array calculated by the electro-thermal method from 9:40 to 14:11 is 0.17 GJ less than that by the conventional method.

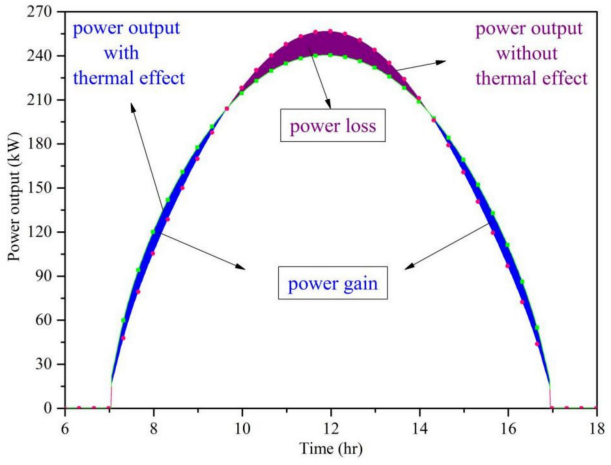

Figure 6. Thermal effect on the power output the winter solstice.

Figures 7 and 8 reveal the thermal characteristics of the solar array on the winter solstice. It can be seen that the temperature distribution which is consistent with the solar radiation distribution is uneven on the solar array, leading to dramatic variation of the photovoltaic efficiency. The temperature of the solar array varies from ~213 to ~315 K at 8:30 and from ~219 to ~339 K at 12:00. Meanwhile, the efficiency of the solar array shows a variation from 0.118 to 0.177 at 8:30 and from 0.104 to 0.177 at 12:00.

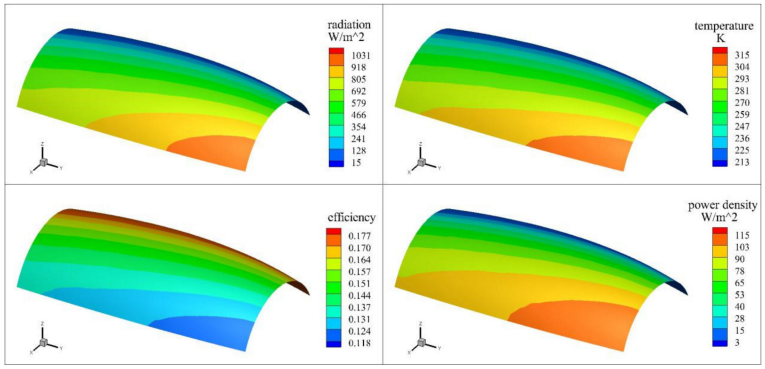

Figure 7. Thermal and energy characteristics of the solar array on the winter solstice at 8:30.

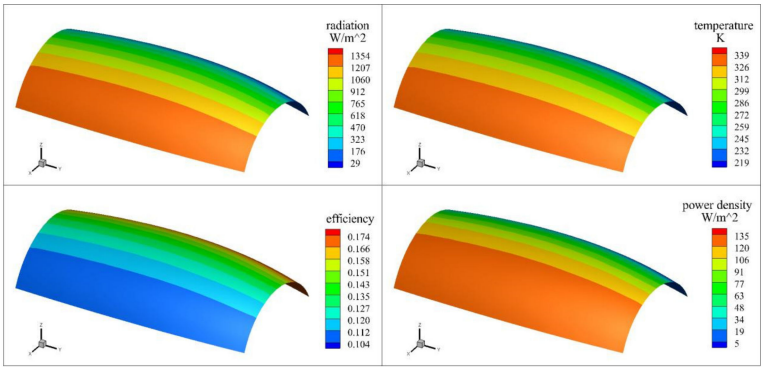

Figure 8. Thermal and energy characteristics of the solar array on the winter solstice at 12:00.

4.2. Energy Supply System Optimization

Five cases of the solar array layout are listed in Table 3. The energies generated in these cases are listed in Table 4.

Table 3. Solar array layout with different cases.

Case	Length	Center Angle	Area
case 1	0.3–0.7 *L*	130°	3055 m^2
case 2	0.25–0.7 *L*	114°	3017 m^2
case 3	0.2–0.7 *L*	104°	3000 m^2
case 4	0.2–0.8 *L*	90°	2971 m^2
case 5	0.1–0.8 *L*	80°	2933 m^2

Table 4. Energy generation on the winter solstice with different cases.

Case	Energy Generated by the Solar Array (GJ)	
	With Thermal Effect	Without Thermal Effect
case 1	6.28	6.26
case 2	6.21	6.12
case 3	6.19	6.04
case 4	6.16	5.92
case 5	6.14	5.83

Helium temperature is an important factor representing the thermal behavior of an airship and should be controlled in an appropriate range to avoid accidents. Therefore, helium temperature was treated as an optimization parameter in this paper. Figure 9 shows the helium temperature variations under different optimization cases on the summer solstice. It is shown that, on the summer solstice, the maximum helium temperatures are

253.8 K for case 1, 254.1 K for case 2, 254.3 K for case 3, 254.5 K for case 4, and 254.5 K for case 5.

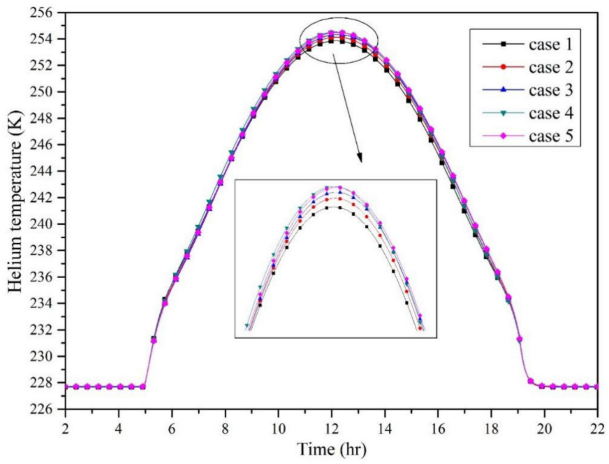

Figure 9. Helium temperature on the summer solstice.

The solar array layout shows great effect on the thermal characteristics. Due to the uneven distributions of solar radiation, the temperature differences of different parts of the solar array are evident. The serious temperature difference distribution on the solar array has a negative effect on the operation life of the solar array and even threatens the safety of the HAA. Therefore, it is necessary to consider the temperature difference of the solar array during the design process. Figure 10 depicts the maximum temperature differences of the solar array on the winter solstice and summer solstice. It can be seen that, on the winter solstice, the maximum temperature difference of the solar array varies slightly under different optimization cases. The temperature difference between different optimization cases is about 10 K. However, on the summer solstice, the variation of the maximum temperature difference of the solar array under different optimization cases can be as high as 35 K.

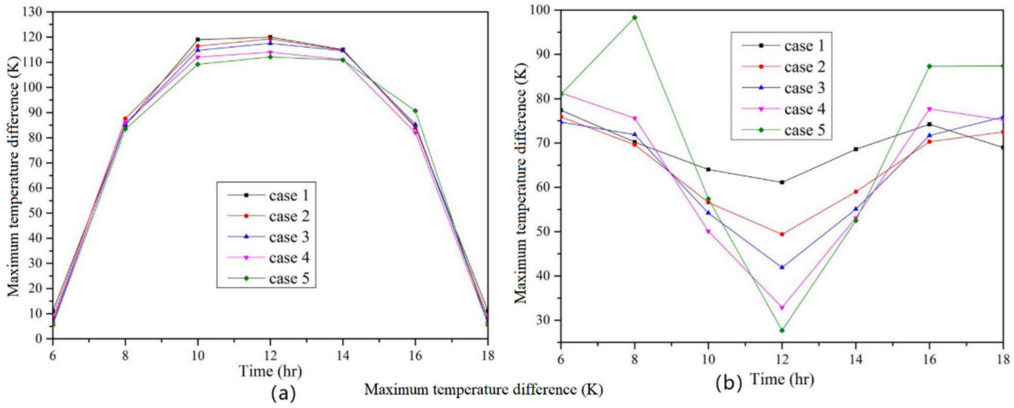

Figure 10. Maximum temperature differences of solar array. (**a**) On the winter solstice; (**b**) on the summer solstice.

The phenomenon was correlated with the solar radiation and downward IR distributions from the atmosphere. On the winter solstice, the maximum solar radiation is located on the dayside of the solar array close to the horizontal central plane of the airship. On the summer solstice, the maximum solar radiation is located on top of the solar array close to the vertical central plane of the airship. The equivalent sky temperature at stratosphere, which is as low as 100 K all through a year, can be considered as a constant heat sink to the

solar array because of the downward atmospheric IR. Therefore, the maximum temperature difference on the winter solstice is much higher than that on the summer solstice.

Considering the electric energy supply and thermal behaviors of helium and the solar array are comprehensive, case 3 was selected as the optimized design scheme. Table 5 shows the mass components of the airship.

Table 5. Effect of solar array absorptivity on mass composition.

Component	Mass (kg)		Improve
	α_{sa} = 0.93	α_{sa} = 0.56	
Envelope	1520	1520	–
Propulsion system	368.5	368.5	–
Solar array	3000	2578	−14.1%
RFC	2474	2460	−0.6%
Payload	1977.5	2075.5	5%

The mass of the RFC system is related to the power output of the solar array and energy consumption. While the mass of the propulsion system is determined by maximum wind speed. The design parameters of the propulsive unit can keep the airship with spot hovering capacity at 20 km in 20 m/s wind. The drag coefficient of the airship is ~0.05 [21]. According to the volume and the density of the ambient air, the maximum power of the propulsive unit is ~48 kW. Therefore, the total mass of the propulsive unit is ~368.5 kg.

It can be seen that mass of the energy supply system, including photovoltaic array and RFC, occupies a large proportion of the total mass. The low solar absorptivity of the solar array can improve the energy output and decrease the area of the solar array and the total mass of the energy supply system. Therefore, the effective load of the airship can be improved. If the solar array absorptivity is reduced from 0.93 to 0.56, the center angle can be decreased from 104° to 90° and the solar array area can drop to 2578 m^2. Thus, the decrease of solar array absorptivity is conducive to improve the economic benefits of the airship application.

5. Conclusions

An electro-thermal model of HAAs is established to study the energy system under actual operational conditions. Based on which, an optimization method considering thermal effect is proposed to design and optimize the energy supply system of HAAs.

Thermal effects on the power output and energy generation of the solar array are unneglectable in the design of energy supply systems for HAAs. In this optimization approach, the thermal behaviors of the solar powered airship are also treated as optimization requirements. The solar absorptivity of the solar array shows negative effects on the energy output. An optimized energy supply system can reduce the maximum temperature difference of the solar array by about 20 K and improve the payload of the airship by up to 5%. It is believed that this work can benefit the optimization design of energy supply systems for HAAs.

Author Contributions: Conceptualization, D.X.; methodology, Q.D. and D.X.; software and data curation, D.X.; formal analysis and investigation, Q.D., D.X. and X.F.; writing—original draft preparation, Q.D. and D.X.; writing—review and editing, Q.D., X.F. and Y.Z.; project administration and funding acquisition, Q.D. All authors have read and agreed to the published version of the manuscript.

Funding: This research was funded by "National Natural Science Foundation of China, grant number 52006100", "Natural Science Foundation of Jiangsu Province, grant number BK20190469" and "the Research Fund of Key Laboratory of Aircraft Environment Control and Life Support, MIIT, Nanjing University of Aeronautics and Astronautics, grant number KLAECLSE-201905". Acknowledgements to Yuanyuan Zhou for improving the English writing.

Data Availability Statement: The data presented in this study are available on request from the corresponding author.

Conflicts of Interest: The authors declare no conflict of interest.

References

1. Androulakakis, S.P.; Jud, R. Status and plans of high altitude airship (HAATM) program. In Proceedings of the AIAA lighter-than-Air Systems Technology (LTA) Conference, Daytona Beach, FL, USA, 25–28 March 2013.
2. Gonzalo, J.; López, D.; Domínguez, D.; García, A.; Escapa, A. On the capabilities and limitations of high altitude pseudo-satellites. *Prog. Aerosp. Sci.* **2018**, *98*, 37–56. [CrossRef]
3. Ceruti, A.; Gambacorta, D.; Marzocca, P. Unconventional hybrid airships design optimization accounting for added masses. *Aerosp. Sci. Technol.* **2018**, *72*, 164–173. [CrossRef]
4. Lv, M.; Li, J.; Du, H.; Zhu, W.; Meng, J. Solar array layout optimization for stratospheric airships using numerical method. *Energy Convers. Manag.* **2017**, *135*, 160–169. [CrossRef]
5. Garg, A.; Burnwal, S.; Pallapothu, A.; Alawa, R.; Ghosh, A. Solar Panel Area Estimation and Optimization for Geostationary Stratospheric Airships. In Proceedings of the 11th AIAA Aviation Technology, Integration, and Operations (ATIO) Conference, Virginia Beach, VA, USA, 20–22 September 2011.
6. Liu, Q.; Yang, Y.; Cui, Y.; Cai, J. Thermal performance of stratospheric airship with photovoltaic array. *Adv. Space Res.* **2017**, *59*, 1486–1501. [CrossRef]
7. Li, J.; Lv, M.; Tan, D.; Zhu, W.; Sun, K.; Zhang, Y. Output performance analyses of solar array on stratospheric airship with thermal effect. *Appl. Therm. Eng.* **2016**, *104*, 743–750. [CrossRef]
8. Alam, M.I.; Pant, R.S. Multidisciplinary approach for solar area optimization of high altitude airships. *Energy Convers. Manag.* **2018**, *164*, 301–310. [CrossRef]
9. Kayhan, Ö. A thermal model to investigate the power output of solar array for stratospheric balloons in real environment. *Appl. Therm. Eng.* **2018**, *139*, 113–120. [CrossRef]
10. Zhu, W.; Xu, Y.; Li, J.; Du, H.; Zhang, L. Research on optimal solar array layout for near-space airship with thermal effect. *Sol. Energy* **2018**, *170*, 1–13. [CrossRef]
11. Zhu, W.; Xu, Y.; Du, H.; Zhang, L.; Li, J. Transmittance optimization of solar array encapsulant for high-altitude airship. *Renew. Energy* **2018**, *125*, 796–805. [CrossRef]
12. Wang, X.; Li, Z.; Zhang, Y. Model for Predicting the Operating Temperature of Stratospheric Airship Solar Cells with a Sup-port Vector Machine. *Energies* **2021**, *14*, 1228.
13. Colozza, A.; Dolce, J. *Initial Feasibility Assessment of a High Altitude Long Endurance Airship*; NASA: Washington, DC, USA, 2003; NASA/CR-212724.
14. Knaupp, W.; Mundschau, E. Solar electric energy supply at high altitude. *Aerosp. Sci. Technol.* **2004**, *8*, 245–254. [CrossRef]
15. Li, G.; Ma, D.; Yang, M. Research of near space hybrid power airship with a novel method of energy storage. *Int. J. Hydrogen Energy* **2015**, *40*, 9555–9562. [CrossRef]
16. Smith, T.; Trancossi, M.; Vucinic, D.; Bingham, C.; Stewart, P. Primary and Albedo Solar Energy Sources for High Altitude Persistent Air Vehicle Operation. *Energies* **2017**, *10*, 573. [CrossRef]
17. Yang, X.; Liu, D. Conceptual Design of Stratospheric Airships Focusing on Energy Balance. *J. Aerosp. Eng.* **2018**, *31*, 04017094. [CrossRef]
18. Xing, D.; Dai, Q.; Liu, C. Thermal characteristics and output power performances analysis of solar powered stratospheric air-ships. *Appl. Therm. Eng.* **2017**, *123*, 770–781. [CrossRef]
19. Skoplaki, E.; Palyvos, J.A. On the temperature dependence of photovoltaic module electrical performance: A review of efficiency/power correlations. *Sol. Energy* **2009**, *83*, 614–624. [CrossRef]
20. Harada, K.; Eguchi, K.; Sano, M.; Sasa, S. Experimental study of thermal modeling for stratospheric platform airships. In Proceedings of the AIAA's 3rd Annual Aviation Technology, Integration, and Operations (ATIO) Forum, Denver, CO, USA, 17–19 November 2003.
21. Lee, S.; Bang, H. Three-Dimensional Ascent Trajectory Optimization for Stratospheric Airship Platforms in the Jet Stream. *J. Guid. Control Dyn.* **2007**, *30*, 1341–1351. [CrossRef]